Biosensors and Bioelectronics 25 (2010) 1212–1216

Contents lists available at ScienceDirect

Biosensors and Bioelectronics

journal homepage: www.elsevier.com/locate/bios

Short communication

A biosensor based on photonic crystal surface waves with an independent registration of the liquid refractive index

Valery N. Konopsky*, Elena V. Alieva

Institute of Spectroscopy, Russian Academy of Sciences, Troitsk, Moscow region, 142190, Russia

ARTICLE INFO

Article history:
Received 19 June 2009
Received in revised form 6 September 2009
Accepted 7 September 2009
Available online 18 September 2009

Keywords:
Label-free optical biosensors
Photonic crystal surface waves
Critical-angle refractometry
Biotin–streptavidin binding

ABSTRACT

A high-precision optical biosensor technique capable of independently determining the refractive index (RI) of liquids is presented. Photonic crystal surface waves were used to detect surface binding events, while an independent registration of the critical angle was used for accurate determination of the liquid RI. This technique was tested using binding of biotin molecules to a streptavidin monolayer at low and high biotin concentrations. The attained baseline noise is 5×10^{-13} m/Hz$^{1/2}$ for adlayer thickness changes and 9×10^{-8} RIU/Hz$^{1/2}$ for RI changes.

1. Introduction

Registration of a bounded optical wave propagating along a bioactive surface is the most popular method used in state-of-the-art direct optical biosensor techniques (Fan et al., 2008). In the surface plasmon resonance (SPR) technique (Homola, 2008), this surface-bound wave is a surface plasmon-polariton propagating along a gold or silver surface, while in optical waveguide techniques this wave is a waveguide mode excited in a high refractive index dielectric layer either via the frustrated total internal reflection (TIR) from a low refractive index spacer (Cush et al., 1993) or via a grating coupler, like it takes place in the integrated-optical waveguide technique (Tiefenthaler and Lukosz, 1989; Lukosz, 1995). For each of these techniques, an evanescent field produced by the optical wave (with penetration depth in water ~100 nm) is sensitive not only to surface-bound biomolecular interactions but also to changes in the volume refractive index (RI) caused by variations in liquid temperature and composition. Therefore, a need exists for a biosensor technique that would be able to segregate the volume and the surface contributions from analytes in the detected signals. To obtain these two parameters, one needs to detect at least two optical waves with different characteristics (e.g., with different penetration depths) simultaneously.

In the work (Konopsky and Alieva, 2007) we used two photonic crystal surface waves (PC SWs) with large differences in penetration depths in order to simultaneously determine the two desired parameters: liquid RI – n_e and the adlayer thickness – d_a. It should be noted here that it is impossible to obtain a large penetration mode depth in standard waveguides, where a RI of the medium under the waveguide film is larger than the RI of the liquid above the film (Konopsky and Alieva, 2007). Therefore, standard waveguides are limited in their ability to reliably segregate volume and surface contributions from an analyte, because both modes have a similar (small) penetration depth in a liquid ($\leq$100 nm). A large penetration depth in a liquid (>1 μm) can only be obtained using so-called "reverse" waveguides, where RI of the medium under the waveguide film is smaller than the RI of the liquid above the film (Horvath et al., 2002a,b). One-dimensional photonic crystal (1D PC) structures are particularly advantageous as they possess the similar feature (in their band gap regions) as substrates in the "reverse" waveguide, despite the fact that a PC structure consists of media with RIs larger than the RI of the liquid (e.g., seven alternative layers of SiO_2 and Ta_2O_5). The large difference among penetration depth of PC SWs in liquids is the main advantage of biosensors based on dual PC SWs (Konopsky and Alieva, 2007, 2009). This attribute allows for (reliable) segregation of the volume and the surface contributions from an analyte and increases sensitivity of molecule detection. Nevertheless, some doubts about the validity of target values (n_e, d_a) derived and about their mutual interdependence may still arise, since each n_e and d_a values depend on both observed PC SW excitation angles and the both calculated target values n_e and d_a are model-based.

In the study presented here we use a direct measurement of the critical TIR angle to immediately obtain the RI n_e of the liquid under investigation. This approach allows one unknown target value – n_e

* Corresponding author.
E-mail address: konopsky@isan.troitsk.ru (V.N. Konopsky).
URL: http://www.isan.troitsk.ru/dsss/lsss/kvn/ (V.N. Konopsky).

0956-5663/$ – see front matter © 2009 Elsevier B.V. All rights reserved.
doi:10.1016/j.bios.2009.09.011

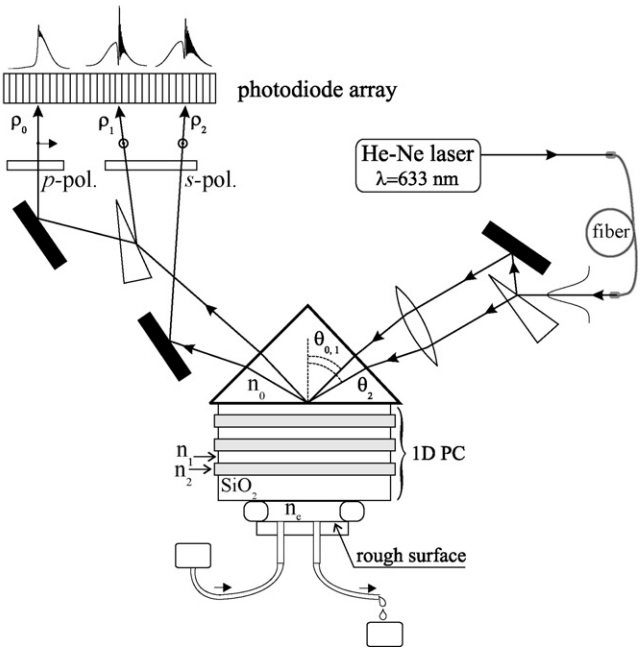

Fig. 1. A sketch of the biosensor. The typical reflection profiles are shown near the photodiode array.

to become model-independent, ultimately increasing the reliability and integrity of results.

2. Materials and methods

2.1. PC SW biosensor

A novel biosensor with an independent registration of the critical angle of the liquid is employed in this study. In Fig. 1 a sketch of the biosensor and typical signals from the photodiode array are shown. A circular-polarized laser beam from He–Ne laser ($\lambda = 632.8$ nm) is sent to the sensor surface through a polarization-maintaining fiber cable (to improve the quality of a beam profile). The beam is split to excite two *s*-polarized PC SWs existing in this 1D PC structure. After reflection from the sensor surface, the reflection profile of the first beam (which is close to the TIR angle) is recorded for both *s*- and *p*-polarizations, while the second one is recorded for *s*-polarization only. The reason for recording the additional *p*-polarization of the first beam is its use for direct registration of the critical TIR angle of the liquid, which immediately provides us the liquid RI. Moreover, the sharpness of the reflection near the critical angle and the measurement precision of the liquid RI herein are much higher than the ones in standard critical-angle refractometers on uncoated prisms (Konopsky and Alieva, in press).

2.2. Photonic crystal structure

The following 1D PC structure is used in experiments: *substrate* / $(LH)^3L'$/*water*, where L is a SiO_2 layer with thickness $d_1 = 186.4$ nm, H is a Ta_2O_5 layer with $d_2 = 115.2$ nm and L' is a SiO_2 layer with $d_3 = 776.8$ nm. The SiO_2/Ta_2O_5 7-layers structure (started and finished by SiO_2 layers) is deposited by magnetron sputtering. The prism and the glass plate substrate are made from BK-7 glass. The RIs of the substrate, SiO_2, Ta_2O_5 and water at $\lambda = 632.8$ nm, are $n_0 = 1.515$, $n_1 = n_3 = 1.47$, $n_2 = 2.07$ and $n_e = 1.332$, correspondingly.

2.3. Reagents

All biochemicals (except streptavidin) were purchased from Sigma–Aldrich (Germany) and were used immediately after preparation. A dialkoxy aminosilane 3-(2-aminoethylamino) propyldimethoxymethylsilane [molecular weight – 206.36] was used to convert OH-terminated SiO_2 surface to NH_2-terminated (Li et al., 2001). Biotin-X-X-NHS [biotinamidohexanoyl-6-aminohexanoic acid N-hydroxysuccinimide ester; molecular weight – 567.7] dissolved in DMF [N,N-dimethylformamide] was used to biotinylate the amino-terminated surface. The streptavidin from Amersham (UK) [molecular weight M_{str}~60 000] was deposited on the biotinylated surface. The free biotin [vitamin H; molecular weight M_b = 244.31] was used as a test to detect small molecule binding with a streptavidin monolayer. All experiments were carried out in PBS [phosphate-buffered saline; pH = 7.2].

2.4. Sample preparation

Samples were prepared as follows: first, glass slides were processed by ionized water vapor in a plasma cleaner for 5 min. Next, these precleaned slides (with expected OH bonds on the ultra-hydrophilic SiO_2 surface) were immersed in 1% aminosilane solution in 95% acetone/water for 5 min. The glass slides, now with expected NH_2 bonds on the ultra-hydrophobic SiO_2 surface, were then dried by argon and baked in vacuum for 20 min at 50 °C. To biotinylate the NH_2-terminated surface the slides were left overnight in solution, where Biotin-X-X-NHS was dissolved by DMF to concentration 12 mg/mL and then the PBS was added (1:1). Afterwards, the slides with biotinylated surface were sequentially sonicated and thoroughly rinsed with DMF and PBS to remove any excess of Biotin-X-X-NHS.

2.5. Flow cell

The flow cell was made from a glass slide with two holes through which two glass tubes were fitted to serve as inlet and outlet, respectively. An internal surface of this glass slide was frosted to avoid reflection causing an additional interference of the refracted beam (at $\theta < \theta_{TIR}$). The inlet tube was connected to a small tank filled with the solution under investigation. Flow velocity was controlled by an elevation difference of the inlet tank and the outlet end level. The height of the cell was determined by the thickness of a Teflon film, which served as a sealing gasket and as a spacer between the sample and the glass slide. We used the Teflon film with 35 μm thickness and corresponding flow cell volume was 3.5 μL. The dead volume of the flow cell system was approximately 25 μL. Gravity flows of streptavidin or biotin solutions and pure PBS buffer were used with volumetric flow rates up to 1 mL/min.

2.6. Data handling

Data from the photodiode array was acquired, processed and presented using homemade software. Changes of the critical angle position P_0 and the resonance peak positions $P_{i(i=1,2)}$ on the photodiode array were converted to changes of the angle parameters ρ_0 and $\rho_i = n_0 \sin(\theta_i)$.

The RI of the liquid was derived as in classical critical-angle Abbe refractometers, through the angle of total internal reflection $\theta_0 = \theta_{TIR}$. The liquid RI is then given by

$$n_e = \rho_0 = n_0 \sin(\theta_0), \quad (1)$$

where n_0 is the RI of the prism in which the critical angle θ_0 is measured.

To obtain the three target values (Δn_e, Δd_a, Δn_a) from the three experimental angular values ($\Delta\rho_0$, $\Delta\rho_1$, $\Delta\rho_2$), one should solve the

next equation:

$$\begin{pmatrix} \Delta\rho_0 \\ \Delta\rho_1 \\ \Delta\rho_2 \end{pmatrix} = \mathbf{M}_{0\,1\,2} \begin{pmatrix} \Delta n_e \\ \Delta d_a \\ \Delta n_a \end{pmatrix}, \tag{2a}$$

where matrix $\mathbf{M}_{0\,1\,2}$ is:

$$\mathbf{M}_{0\,1\,2} = \begin{pmatrix} 1 & 0 & 0 \\ \partial\rho_1/\partial n_e & \partial\rho_1/\partial d_a & \partial\rho_1/\partial n_a \\ \partial\rho_2/\partial n_e & \partial\rho_2/\partial d_a & \partial\rho_2/\partial n_a \end{pmatrix}. \tag{2b}$$

The solution of the Eq. (2a) for the three target values is:

$$\begin{pmatrix} \Delta n_e \\ \Delta d_a \\ \Delta n_a \end{pmatrix} = (\mathbf{M}_{0\,1\,2})^{-1} \begin{pmatrix} \Delta\rho_0 \\ \Delta\rho_1 \\ \Delta\rho_2 \end{pmatrix}. \tag{3}$$

This equation is solvable when $\det(\mathbf{M}_{0\,1\,2}) \neq 0$. Unfortunately, at small adlayer thickness, $\partial\rho_1/\partial d_a \simeq C \times (\partial\rho_1/\partial n_a)$ and $\partial\rho_2/\partial d_a \simeq C \times (\partial\rho_2/\partial n_a)$ with approximately the same proportionality constant C in both cases. Thereby, the second and the third columns in matrix $\mathbf{M}_{0\,1\,2}$ (see (2b)) are not linear independent:

$$\begin{pmatrix} 0 \\ \partial\rho_1/\partial d_a \\ \partial\rho_2/\partial d_a \end{pmatrix} \simeq C \times \begin{pmatrix} 0 \\ \partial\rho_1/\partial n_a \\ \partial\rho_2/\partial n_a \end{pmatrix} \tag{4}$$

and, therefore (see, e.g., Korn and Korn, 1968), $\det(\mathbf{M}_{0\,1\,2}) \simeq 0$ at small adlayer thicknesses (and, furthermore, $\det(\mathbf{M}_{0\,1\,2}) \to 0$ while $d_a \to 0$). As a result, the solutions (3) for *the three* target values (including Δn_a) are very noisy and unstable when d_a is small (because each solution is a small residual after subtraction of large values with $\det(\mathbf{M}_{0\,1\,2})$ in denominator).

If we postulate that $n_a \simeq$ const, the matrix $\mathbf{M}_{0\,1\,2}$ may be diminished to $\mathbf{M}_{0i\,(i=1\,\text{or}\,2)}$ and the Eqs. (2a) and (2b) become the next:

$$\begin{pmatrix} \Delta\rho_0 \\ \Delta\rho_i \end{pmatrix} = \begin{pmatrix} 1 & 0 \\ \partial\rho_i/\partial n_e & \partial\rho_i/\partial d_a \end{pmatrix} \begin{pmatrix} \Delta n_e \\ \Delta d_a \end{pmatrix}. \tag{5}$$

It may be noted here that the model solution, where the matrix $\mathbf{M}_{0\,1\,2}$ is diminished to $\mathbf{M}_{1\,2}$ ($n_a \simeq$ const):

$$\begin{pmatrix} \Delta\rho_1 \\ \Delta\rho_2 \end{pmatrix} = \begin{pmatrix} \partial\rho_1/\partial n_e & \partial\rho_1/\partial d_a \\ \partial\rho_2/\partial n_e & \partial\rho_2/\partial d_a \end{pmatrix} \begin{pmatrix} \Delta n_e \\ \Delta d_a \end{pmatrix}, \tag{6}$$

has been exploited by us early (see Konopsky and Alieva, 2007, Eq. (2)).

In the present article, to derive the changes of the adlayer thickness from the changes of the resonance angle i and Δn_e, we use the solution of (5):

$$\begin{pmatrix} \Delta n_e \\ \Delta d_a \end{pmatrix} = (\mathbf{M}_{0i})^{-1} \begin{pmatrix} \Delta\rho_0 \\ \Delta\rho_i \end{pmatrix} \tag{7}$$

and obtain the next relations for *the two* target values:

$$\Delta n_e = \Delta\rho_0 \tag{8a}$$

$$\Delta d_a = \frac{\Delta\rho_i - (\partial\rho_i/\partial n_e)\Delta n_e}{(\partial\rho_i/\partial d_a)}. \tag{8b}$$

The coefficients $(\partial\rho_i/\partial n_e)$ and $(\partial\rho_i/\partial d_a)$ are able to be obtained, for example, from a theoretical simulation of the real 1D PC structure. The Δn_e and Δd_a data presented below were derived using the Eqs. (8a) and (8b), with the coefficients, which mean values are approximately equal: $\langle(\partial\rho_2/\partial n_e)\rangle \simeq 0.053$, $\langle(\partial\rho_2/\partial d_a)\rangle \simeq 0.057$ [1/ μm]. Precise values of these coefficients slightly depend on n_e and d_a and were derived for each particular point using dispersion relations of PC SWs (e.g., given in Yeh et al., 1977). Note that Δn_e does not depend (see Eqs. (8a) and (1)) on these coefficients and, therefore, does not depend on the model of 1D PC structure.

3. Results

3.1. Streptavidin monolayer deposition

Streptavidin (diluted in PBS to a concentration of $c_{\text{str}} = 12$ μg/mL) was run through the flow cell with a volumetric flow rate $v_{\text{str}} = 0.3$ mL/min. Fig. 2 illustrates that the increase of the adlayer thickness due to immobilization of streptavidin on a biotinylated surface (top left) occurs with kinetics different from those of the RI change of buffer during injection (see bottom left). This fact indicates that the volume and surface contributions from an analyte are indeed separated into different registration channels.

3.2. Biotin binding to the streptavidin monolayer

The right side of Fig. 2 presents the adlayer thickness changes observed during free biotin binding to the streptavidin monolayer (top right) and the RI changes of the analyte (bottom right) during this biotin solution injection. Biotin (in a concentration of $c_{\text{b(low)}} = 0.9$ μg/mL) was injected into PBS running through the flow cell with volumetric flow rate $v_{\text{b}} = 0.4$ mL/min. One can see that the biosensor reliably detects the increase in streptavidin monolayer thickness at free biotin binding ($\Delta d_a \simeq 0.45$ Å).

It should be noted here that the behaviour of the streptavidin–biotin complex appeared to depend on the concentration of the injected biotin solution. In several published experimental analyses, the thickness of the streptavidin–biotin complex was slowly and monotonically decreased after an initial sharp increase (Zybin et al., 2005; Konopsky and Alieva, 2007). We found that such behaviour may take place in the presence of an excess concentration of free biotin. To illustrate this point, we injected free biotin at high concentration $c_{\text{b(high)}} = 80$ μg/mL in the flow cell. Indeed, after a short initial increase, the thickness of the streptavidin monolayer was monotonically decreased as shown in Fig. 3. One possible explanation for this process may be the fact that free biotin (at high concentrations) acts as a competitor for streptavidin sites that are bound to the surface (Green and Toms, 1973), i.e., elution of the streptavidin molecules from the surface may be taking place.

The detected increase in the physical thickness of the streptavidin monolayer $\Delta d_a \simeq 0.45$ Å (upon injection of low biotin concentrations, see Fig. 2, top right) is in agreement with previously published data, where an increase in optical thickness (i.e., physical thickness of the adlayer multiplied by the adlayer RI) $\Delta(d_a n_a) \simeq 0.6$–$0.7$ Å was measured by reflectometric interference spectroscopy technique (Piehler et al., 1996). Taking into account the refractive index of the adlayer $n_a = 1.43$, which was used in our computations, we obtain a reasonable agreement in measured values.

4. Discussion

4.1. RI sensitivity and baseline noises

The sensitivity of a sensor to the liquid RI can be expressed as a product of two terms (Homola, 2008):

$$S_{\text{RI}} = \frac{\partial I}{\partial\rho}\frac{\partial\rho}{\partial n_e} = \frac{\partial R_p}{\partial\rho}\frac{\partial\rho}{\partial n_e}, \tag{9}$$

where the derivative of the detected laser light intensity I as a function of $\rho = n_0 \sin(\theta)$ is taken as the sharpness of the reflection

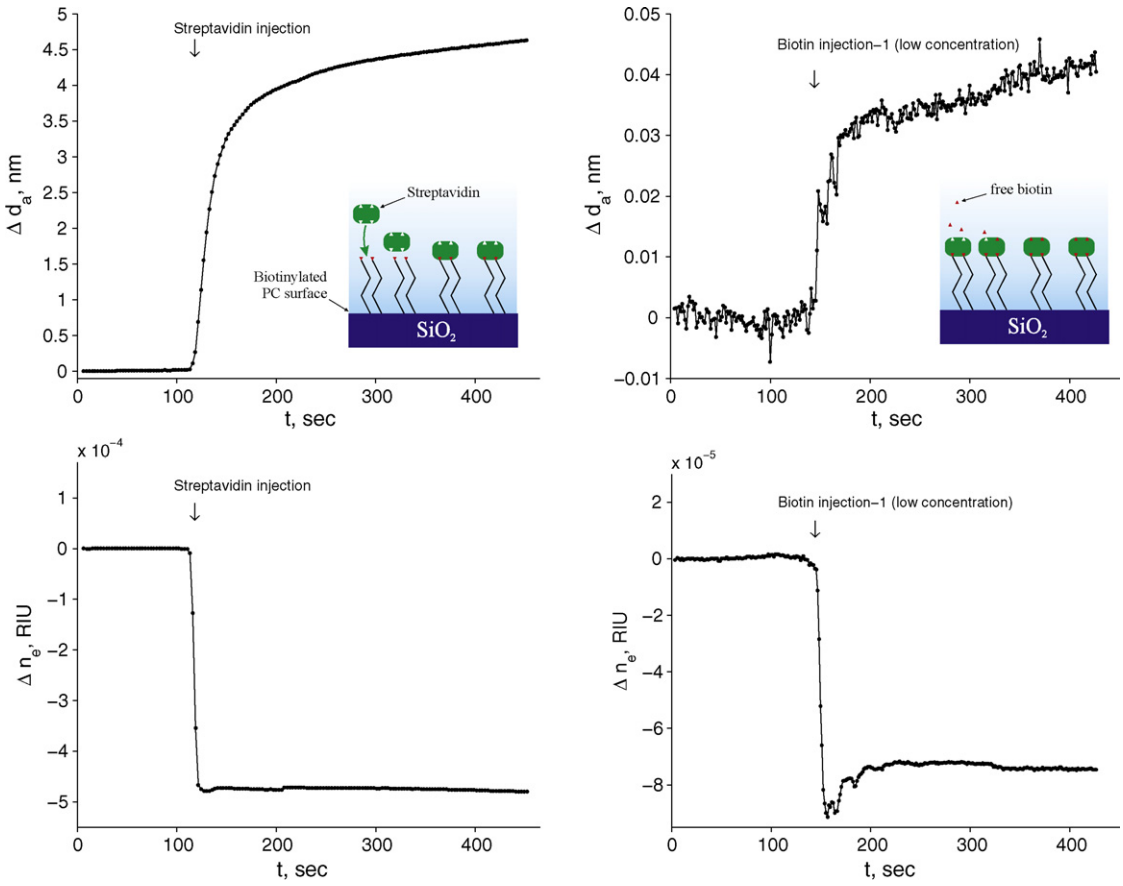

Fig. 2. Immobilization of streptavidin on a biotinylated surface (top left) with subsequent binding of free biotin to this streptavidin monolayer (top right) and corresponding changes of RI of the buffer during these injections (bottom). The measurement time was 1 s per point (no posterior data averaging and smoothing). In color inserts corresponding processes are illustrated. (For interpretation of the references to color in this figure legend, the reader is referred to the web version of the article.)

coefficient R near the critical angle ρ_0 in our case (and for Abbe refractometers). The second term is equal to unity at $\rho = \rho_0$ in the presented system like in classical critical-angle Abbe refractometers: $\partial\rho/\partial n_e = 1$, while in SPR-based RI sensors this term is slightly larger than unity: $\partial\rho_{SPR}/\partial n_e \simeq 1.15$ (for the gold film in the water at the $\lambda = 632.8$ nm wavelength).

A high sensitivity of the RI detection in the presented method arises from the fact that the sharpness of the reflection near the critical angle (see its shape in Fig. 1, at the top left corner) is much higher in our system than both in SPR-based systems and in standard critical-angle refractometers on uncoated prisms. In the critical-angle Abbe refractometer $\max(\partial R_s/\partial\rho) \simeq 200$ for s-polarization and $\max(\partial R_p/\partial\rho) \simeq 250$ for p-polarization (in the best case). In SPR-based sensors the maximum sharpness of an SPR curve (near its half-width points) is $\max(\partial R_p/\partial\rho_{SPR})$~20–40 only (for the gold film in the water at the same wavelength), while in the presented system $\max(\partial R_p/\partial\rho)$ is about 1000, and may be even higher if additional SiO_2/Ta_2O_5 layer pairs would be added.

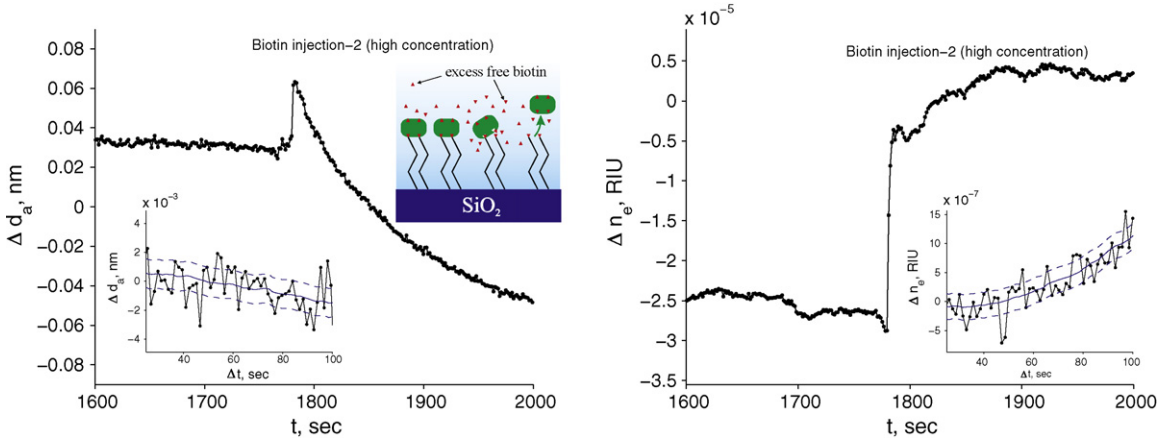

Fig. 3. The injection of a high concentration of free biotin: changes in the thickness of the streptavidin–biotin complex (left) and the corresponding change of RI of the buffer (right). In color insert the possible corresponding process is illustrated. Enlarged views of the baseline noises are presented as inserts at the bottom. (For interpretation of the references to color in this figure legend, the reader is referred to the web version of the article.)

Such a high value of S_{RI} leads to the decrease of the baseline noise arising from the laser light intensity noise δI because $\delta n_e \sim \delta I/S_{RI}$ – see, e.g. Homola (2008). But, unfortunately, other types of δn_e noises, such as a thermodynamic noise of the liquid RI arising from temperature fluctuations does not depend on the S_{RI} value. Enlarged views of the experimental baseline noises are presented as inserts in corresponding parts of Fig. 3. The time of one point measurement was about 1 s, including the light accumulation time by the diode array, which was equal 0.3 s in each point. Taking into account the root dependence of a baseline noise on time we obtain the next values of the attained noise floor from bottom inserts in Fig. 3: $\delta n_e = 9 \times 10^{-8}$ RIU/Hz$^{1/2}$ and $\delta d_a = 5 \times 10^{-13}$ m/Hz$^{1/2}$. The limit of detection is usually defined as three standard deviation of the baseline noise (Analytical Methods Committee, 1987).

4.2. Assumptions and limitations in the presented registrations system

It has been already noted that the system presented here, wherein three independent angle parameters are recorded, may also be used to experimentally determine the adlayer RI as the third calculated value (together with the adlayer thickness and the RI of the liquid). However, as was pointed above, after the Eq. (3), this type of adlayer RI determination yields precise ($\leq$0.01) and reliable values only when considering rather large adlayer optical thicknesses. We have experimentally found that all the three target values became very noisy indeed (not shown), when we tried to derive adlayer RI from obtained data for small adlayer thicknesses. There is a rather fundamental reason behind this limitation, which will be discussed elsewhere.

To avoid this type of noise (arising due to smallness of $\det(\mathbf{M}_{012})$) we have used only one *s*-polarized wave (at ρ_2) with one *p*-polarized wave (at ρ_0) in the presented study. Therefore, our analysis has been based on the assumption of a homogeneous adlayer with constant n_a and on the assumption of homogeneous variations of the liquid RI. It should be noted that these assumptions may lead to false conclusions in the case of some exotic and non-homogeneous spatial distribution of Δn_e variations. For example, if the liquid RI changes within the range that can be seen only by the deeply penetrating *p*-polarized evanescent wave, but not by the *s*-polarized evanescent wave – i.e., if some Δn_e variation occurs at around $L_e \sim$5–10 μm away from the interface and above, but does not occur below (near the interface) – then a false (reverse) Δd_a will be created by the Eq. (8b). While an "ideal" registration system (which can detect the real variation of Δn_a) would produce (in this exotic case) not the reverse adlayer thickness variation, but a reverse variation of the adlayer RI: $\Delta n_a = -\Delta n_e$ inside the thickness $d_a = L_e$.

5. Conclusions

In this paper we have proposed and experimentally tested a new biosensor technique capable of direct and model-independent determination of the RI of a liquid. The liquid RI is determined by measuring the critical angle for *p*-polarization of the laser beam, while the *s*-polarization is used for the excitation of the adlayer-thickness-sensitive PC SW. The attained noise floor of the RI baseline is $\delta n_e = 9 \times 10^{-8}$ RIU/Hz$^{1/2}$, while the baseline noise of the adlayer thickness is $\delta d_a = 5 \times 10^{-13}$ m/Hz$^{1/2}$ = 0.5 pm/Hz$^{1/2}$. The potential to record surface and volume events independently may be an important advantage in a number of applications where temperature and composition of the liquid under study may vary over a wide range.

Acknowledgments

This work was financially supported by the Grant 09-02-00366-a from the Russian Foundation for Fundamental Researches. The authors would like to thank D. Klinov for his help in sample preparation.

References

Analytical Methods Committee, 1987. Analyst 112, 199–204.
Cush, R., Cronin, J., Stewart, W., Maule, C., Molloy, J., Goddard, N., 1993. Biosens. Bioelectron. 8 (7–8), 347–353.
Fan, X., White, I.M., Shopoua, S.I., Zhu, H., Suter, J.D., Sun, Y., 2008. Anal. Chim. Acta 620 (1–2), 8–26.
Green, N.M., Toms, E.J., 1973. Biochem. J. 133 (4), 687–698.
Homola, J., 2008. Chem. Rev. 108 (2), 462–493.
Horvath, R., Lindvold, L., Larsen, N., 2002a. Appl. Phys. B-Lasers Opt. 74 (4–5), 383–393.
Horvath, R., Pedersen, H., Larsen, N., 2002b. Appl. Phys. Lett. 81 (12), 2166–2168.
Konopsky, V.N., Alieva, E.V., 2007. Anal. Chem. 79 (12), 4729–4735.
Konopsky, V.N., Alieva, E.V., Sens. Actuator B-Chem., in press.
Konopsky, V.N., Alieva, E.V., 2009. In: Rasooly, A., Herold, K.E. (Eds.), Biosensors and Biodetection, Methods and Protocols, Volume 1: Optical-Based Detectors. Vol. 503 of Springer Protocols: Methods in Molecular Biology. Humana Press, Totowa, NJ, USA, Ch. 4, pp. 49–64.
Korn, G.A., Korn, T.M., 1968. Mathematical Handbook.
Li, J., Wang, H., Zhao, Y., Cheng, L., He, N., Lu, Z., 2001. Sensors 1, 53–59.
Lukosz, W., 1995. Sens. Actuator B-Chem. 29 (1–3), 37–50.
Piehler, J., Brecht, A., Gauglitz, G., 1996. Anal. Chem. 68 (1), 139–143.
Tiefenthaler, K., Lukosz, W., 1989. J. Opt. Soc. Am. B-Opt. Phys. 6 (2), 209–220.
Yeh, P., Yariv, A., Hong, C.-S., 1977. J. Opt. Soc. Am. 67 (4), 423–438.
Zybin, A., Grunwald, C., Mirsky, V.M., Kuhlmann, J., Wolfbeis, O.S., Niemax, K., 2005. Anal. Chem. 77, 2393–2399.